

## Singlet-triplet spin blockade and charge sensing in a few-electron double quantum dot

A. C. Johnson, J. R. Petta, and C. M. Marcus

*Department of Physics, Harvard University, Cambridge, Massachusetts 02138, USA*

M. P. Hanson and A. C. Gossard

*Department of Materials, University of California, Santa Barbara, California 93106, USA*

(Received 8 July 2005; published 5 October 2005)

Singlet-triplet spin blockade in a few-electron lateral double quantum dot is investigated using simultaneous transport and charge-sensing measurements. Transport from the (1,1) to the (0,2) electron occupancy states is strongly suppressed relative to the opposite bias [(0,2)–(1,1)]. At large bias, spin blockade ceases as the (0,2) triplet state enters the transport window, giving a direct measure of exchange splitting of the (0,2) state as a function of magnetic field. A simple model for current and steady-state charge distribution in spin-blockade conditions is developed and found to be in excellent agreement with experiment. Three other transitions [(1,1)–(2,0), (1,3)–(2,2), and (1,3)–(0,4)] exhibit spin blockade while other nearby transitions and opposite bias configurations do not, consistent with simple even-odd shell filling.

DOI: 10.1103/PhysRevB.72.165308

PACS number(s): 73.21.La, 72.25.–b, 73.63.Kv

## I. INTRODUCTION

Great progress has been made in engineering solid-state systems that exhibit quantum effects, providing tools for probing fundamental problems in many-body physics as well as device technologies. In semiconductor quantum dots, small numbers of confined electrons can be manipulated using electrostatic gates with surprising ease.<sup>1–3</sup> For the case of two electrons in the dot (quantum dot “helium”), Pauli exclusion and exchange induce a splitting between the spin singlet and triplet states that can be controlled by gates and magnetic fields.<sup>4</sup> In double dots, a consequence of this splitting is current rectification, in which transitions from the (1,1) to the (0,2) state (ordered pairs indicate electron occupancy in each dot) is blocked, while the opposite bias case, involving transitions from (0,2) to (1,1) proceeds freely. Rectification is a direct consequence of spin selection rules.<sup>5</sup>

Spin blockade of this type can be understood by considering positive and negative bias transport in a double dot containing one electron in the right dot, as indicated in Figs. 1(b) and 1(c). An electron of any spin can enter the left dot, making either a (1,1) singlet or triplet, these states being nearly degenerate for weak interdot tunneling.<sup>6</sup> In contrast, the right dot can accept an electron only to make a (0,2) singlet. At positive bias [Fig. 1(b)] current can flow: an electron enters the right dot to make a (0,2) singlet, tunnels to the (1,1) singlet, and escapes. At negative bias [Fig. 1(c)], an electron can enter the left dot and form a (1,1) triplet state. A transition from the (1,1) triplet to the (0,2) singlet is forbidden by conservation of spin and transport is blocked. Recent measurements have shown rich behavior of electrons circumventing the blockade, due to hyperfine interactions between the electron and nuclear spins.<sup>7,8</sup>

Here we report a detailed investigation of spin blockade through a lateral few-electron double-dot system, measured using both transport and charge sensing by a nearby quantum point contact (QPC) to detect the charge arrangement during blockade.<sup>9</sup> We observe that transmission through double-dot states containing two electrons is strongly rectified, while

transmission of the first electron is symmetric in bias. Negative-bias blockade is truncated when the (0,2) triplet state enters the bias window, allowing the magnetic field dependence of the singlet-triplet splitting to be measured from both transport and charge sensing. Simple rate-equation models for transport and charge distributions reproduce key features in both types of data, and allow relative tunnel rates to be extracted. Finally, other charge transitions are investigated, up to the second electron in the left dot and the fourth in the right dot. The presence or absence of spin blockade is shown to be consistent with even-odd shell filling.

Spin blockade of transport, arising from a variety of mechanisms, has been investigated previously in quantum dot systems;<sup>3,10</sup> the mechanism responsible for the present spin blockade was investigated in vertical structures in Ref. 5. The lateral, gate-defined structure we investigate has some

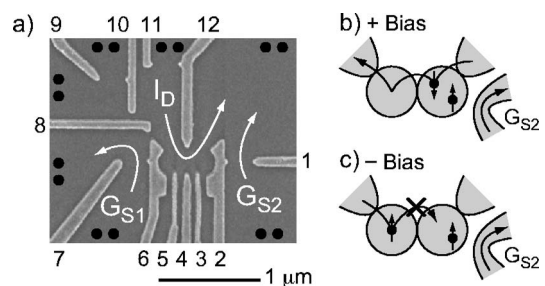


FIG. 1. (a) Electron micrograph of a device identical in design to the one measured. Gates 2–6 and 12 define the double dot, 1 and 7 form QPC charge sensors, 8 separates the left QPC and double dot current paths, and 9–11 are unused. Black spots (●) denote ohmic contacts. The origin of spin blockade, when the left dot has 0–1 electrons and the right dot 1–2 electrons, is illustrated in (b) and (c). Opposite spins represent a singlet, same spins a triplet. The left dot accepts any spin but the right can only form a spin singlet, blocking negative bias current once the wrong spin occupies the left dot. A charge sensor ( $G_{S2}$ ) also registers the blockade, as a second electron is sometimes in the right dot at positive bias, but not at negative bias.

advantages over vertical structures by allowing independent tuning of all tunnel barriers so that sequential tunneling with arbitrary dot occupations can be explored. QPC charge sensors provide additional information, including the average charge distribution when transport is absent in the spin blockade regime.

## II. EXPERIMENTAL TECHNIQUES

The sample, shown in Fig. 1(a), is fabricated on a GaAs/Al<sub>0.3</sub>Ga<sub>0.7</sub>As heterostructure with two-dimensional electron gas (density  $2 \times 10^{11} \text{ cm}^{-2}$ , mobility  $2 \times 10^5 \text{ cm}^2/\text{V s}$ ) 100 nm below the wafer surface, patterned with Ti/Au top gates. Gates 2–6 and 12 define a double quantum dot in which each dot can be tuned from zero to several electrons.<sup>11</sup> Gates 1 and 7 define QPCs whose conductance is most sensitive to the charge on the right and left dots respectively. Gate 8 isolates the current path of the double dot from the left QPC, while the double dot and right QPC share a common ground. Gates 9–11 are not energized. Current through the double dot ( $I_D$ ) is measured in response to a dc voltage on the left reservoir. A small ac excitation (6  $\mu\text{V}$  at 27 Hz) allows lock-in measurement of differential conductance. Conductances of QPC charge sensors ( $G_{S1,2}$ ) are measured simultaneously with separate lock-in amplifiers (1 nA current bias at 93 and 207 Hz). Base electron temperature is  $T_e \sim 135 \text{ mK}$ , measured from Coulomb blockade diamonds. Two devices were measured and showed qualitatively similar behavior; data from one device are presented.

## III. RESULTS AND DISCUSSION

### A. Transport measurements

Figure 2 shows  $I_D$  at  $\pm 0.5 \text{ mV}$  bias as a function of gate voltages  $V_2$  and  $V_6$ , which primarily control the energy levels in the right and left dots. Figures 2(a) and 2(c) were measured near the conductance resonance of the first electron, with  $(m, n)$  indicating the charge states surrounding the resonance. At positive bias, finite current is measured within two overlapping triangles in gate voltage space, satisfying the inequalities  $\mu_R \geq \varepsilon_R \geq \varepsilon_L \geq \mu_L$  or  $\mu_R \geq \varepsilon_R + E_m \geq \varepsilon_L + E_m \geq \mu_L$ . Here  $\mu_{L,R}$  are the chemical potentials of the leads,  $\varepsilon_{L,R}$  are the energies to add an electron to the ground state of either dot, and the mutual charging energy  $E_m$  is the extra energy to add an electron to one dot with the other dot occupied.<sup>12</sup> The first set of inequalities defines the lower, or *electron triangle*, where, starting at (0,0), an electron hops through the dots from one lead to the other. The second inequalities define the upper, or *hole triangle*, where, starting at (1,1), a hole hops across the dots. Electron and hole processes involve the same three tunneling events, only their order changes. Schematics at the top of Fig. 2 depict the energy level alignments at the vertices of the electron triangle in Fig. 2(a). Within the triangles, current depends primarily on the detuning  $\Delta = \varepsilon_L - \varepsilon_R$  of one-electron states, with a maximum current at  $\Delta = 0$ , demonstrating that interdot tunneling is strongest at low energy loss, consistent with previous studies of inelastic tunneling in double dots.<sup>13</sup> At negative bias [Fig. 2(c)] the triangles flip and current changes

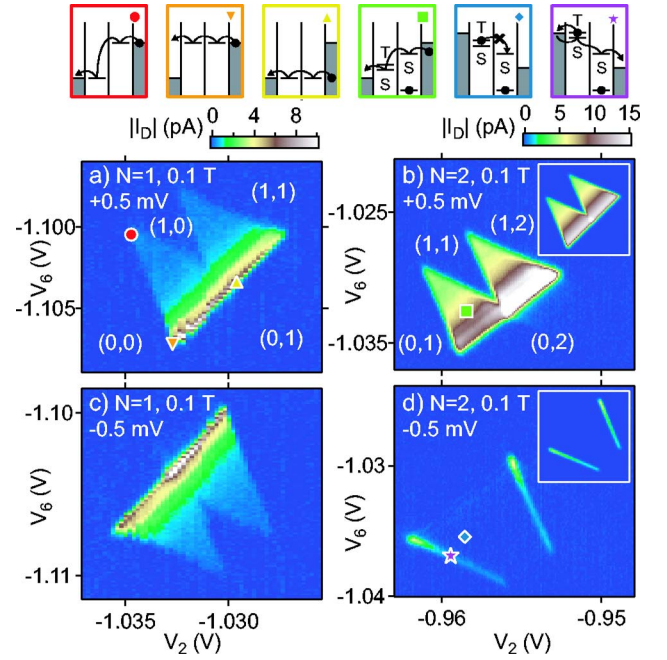


FIG. 2. (Color online) (a) Magnitude of current  $I_D$  as a function of  $V_2$  and  $V_6$  across the (1,0)–(0,1) transition at 0.5 mV bias. Ordered pairs  $(m, n)$  denote electrons on the left ( $m$ ) and right ( $n$ ) dots, with  $N$  total electrons present during interdot tunneling. The red (●), orange (▼), and yellow (▲) diagrams illustrate the level alignments bounding a bias triangle. The same configuration at  $-0.5 \text{ mV}$  bias, (c), shows almost perfect symmetry. (b) and (d) show the equivalent data at the (1,1)–(0,2) transition. Current flows freely at positive bias, as depicted in the green diagram (■). Negative bias current is suppressed by spin blockade (blue diagram, ◆) except on the lower (purple diagram, ★) and upper edges. Insets to (b) and (d) show results of a rate equation model which captures most features of the data (see text).

sign, but otherwise these data mimic the positive bias case [Fig. 2(a)].

The corresponding data with another electron added to the right dot is shown in Figs. 2(b) and 2(d). At positive bias, the data qualitatively resemble the one-electron case. However, at negative bias the current is nearly zero, except along the outermost edges of the electron and hole triangles. Referring to the diagrams above Fig. 2, at positive bias, current proceeds freely from right to left through singlet states (green square). At negative bias, an electron enters the left dot into either the (1,1) singlet or triplet. If it enters the (1,1) singlet, it may continue through the (0,2) singlet. However, once an electron enters the (1,1) triplet, it can neither continue to the right [into the (0,2) singlet] nor go back into the left lead because it is below the Fermi level and the hole it left quickly diffuses away. Thereafter, negative-bias transport requires a spin flip or a second-order spin exchange process with one of the leads. Insofar as these processes are relatively slow, transport in this direction is blocked.

Along the outer edge of the lower (electron) triangle, where transport is observed in the negative-bias direction [Fig. 2(d), purple star], an electron trapped in the (1,1) triplet state is within the thermal window of the left lead and will occasionally exchange with another electron possibly load-

ing the (1,1) singlet, which can then move to the right, through the (0,2) singlet, and contribute to current. An analogous mechanism in the hole channel allows negative-bias current along the upper edge of the hole triangle: with transitions from (1,1) to (1,2) within the thermal window, the blockade created by an occupied (1,1) triplet can be lifted by adding an electron, making a (1,2) state, then removing it, possibly leaving a (1,1) singlet that can contribute to current.

A simple rate-equation model allows the spin-blockade picture to be quantitatively checked against transport data, and also indicates where charge resides in the double dot, which can be compared to charge sensing data. The model takes two degenerate levels in the left dot, representing the (1,1) singlet and triplet states, coupled equally to a thermally broadened left reservoir (i.e., ignoring the extra degeneracy of the triplet)<sup>14</sup> and a single level of the right dot, representing the (0,2) singlet [assuming the (0,2) triplet is energetically inaccessible] coupled to the right reservoir. The singlet levels are coupled by thermally activated inelastic tunneling, with the shape of the  $\Delta=0$  peak inserted to match the positive-bias current data. Temperature, mutual charging energy, and the gate capacitances are determined from measurements. Calculated current is shown in the insets to Figs. 2(b) and 2(d). The model resembles the experimental data, with two minor exceptions: At positive bias, measured current is higher in the hole triangle than the electron triangle, implying that the dot-lead tunnel barriers are, in this case, more transparent with the other dot occupied. Also, the small but finite blockade current is absent in the model, as expected since the model contains only first-order, spin-conserving processes.

### B. Charge sensing measurements

Figure 3 shows the charge sensor data  $G_{S2}$  vs  $V_2$  and  $V_6$ , acquired simultaneously with each panel in Fig. 2. A plane is subtracted from each data set to remove direct coupling between the gates and the QPC, leaving only the effect of the average dot occupations. Away from the bias triangles we see plateaus for each stable charge state, which are used to calibrate the response. In Figs. 3(a) and 3(c), QPC conductance jumps  $\Delta G_R=0.016 e^2/h$  due to a charge in the right dot, and  $\Delta G_L=0.008 e^2/h$  due to the left. These values vary between data sets, but this QPC is always about twice as sensitive to the closer dot.

Within each bias triangle, the sensing signal varies with the fraction of time an electron spends in each charge state. Consider Fig. 3(a), the one-electron positive bias data. As with transport through the dot, charge sensing is primarily dependent on detuning,  $\Delta$ . For small interdot tunneling, the system rests mainly in (0,1), thus at large detuning the sensing signal matches the (0,1) plateau. In the electron triangle, as detuning decreases and interdot tunneling increases, the system spends more time in (1,0) and (0,0). Both increase the right QPC sensor conductance. In the hole triangle, the system accesses (1,0) and (1,1), which, respectively, increase and decrease the right sensing signal.

Assuming the same tunnel rates to the leads in the electron and hole triangles, lead asymmetry can be quantified by

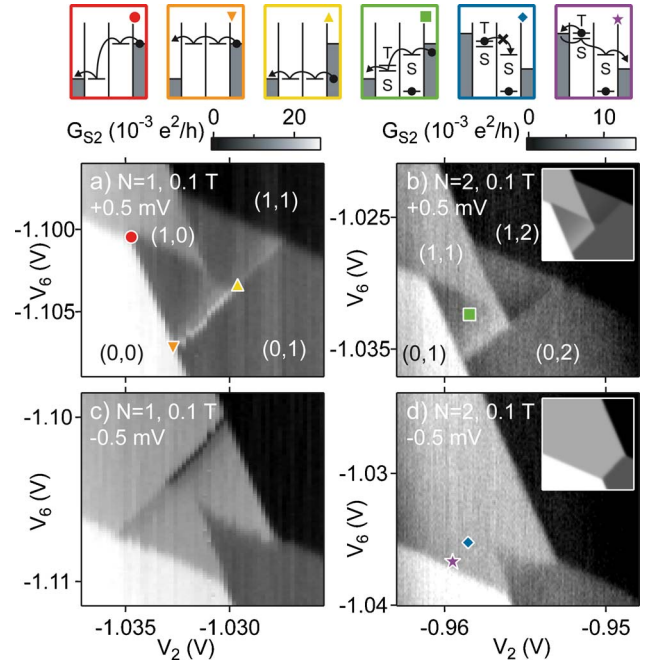


FIG. 3. (Color online) Charge sensor signal  $G_{S2}$  measured simultaneously with each panel of Fig. 2. A plane is subtracted from each panel to remove direct gate-QPC coupling. The first electron, (a) and (c), again shows bias symmetry while the second, (b) and (d), is missing features at negative bias. The model used in Fig. 2 also reproduces the charge sensor data, as shown in the insets to (b) and (d), with slight disagreement due to second-order processes (see text).

comparing the rate-equation model to the sensor signal in the two triangles. At the one-electron transition, the charge sensor signal can be written as a deviation from the (0,1) plateau,  $\Delta G_S = \Delta G_R(p_{10} + p_{00}) - \Delta G_L(p_{10} + p_{11})$ , where  $p_{mn}$  is the occupation probability of charge state  $(m, n)$ . At positive bias, current flows only leftward through each barrier, thus conservation of current gives  $p_{01}^e \Gamma_D = p_{10}^e \Gamma_L = p_{00}^e \Gamma_R$  in the electron triangle and  $p_{01}^h \Gamma_D = p_{10}^h \Gamma_R = p_{11}^h \Gamma_L$  in the hole triangle, where  $\Gamma_D$ ,  $\Gamma_L$ , and  $\Gamma_R$  are the interdot, left, and right barrier tunnel rates. As each set of three probabilities sums to unity, we can calculate each individually {e.g.,  $p_{00}^e = [1 + (\Gamma_R/\Gamma_L) + (\Gamma_R/\Gamma_D)]^{-1}$ }. We define a quantity  $\alpha$  as the ratio of  $\Delta G_S$  in the hole triangle to  $\Delta G_S$  at the same detuning (thus the same  $\Gamma_D$ ) in the electron triangle, which gives  $\alpha = [(S-1)p_{10}^h - p_{11}^h] / [(S-1)p_{10}^e + S p_{00}^e]$ , where  $S$  is the QPC sensitivity ratio  $\Delta G_R/\Delta G_L$ . Inserting the expressions for the occupation probabilities in terms of tunnel rates, we find

$$\alpha = [S - 1 - \Gamma_R/\Gamma_L] / [(S-1)\Gamma_R/\Gamma_L + S]. \quad (1)$$

This expression is independent of  $\Gamma_D$  (and therefore independent of detuning), implying that the line shape of  $\Delta G_S$  as a function of detuning is the same in each triangle, up to an overall positive or negative factor  $\alpha$ . This can be seen qualitatively in Figs. 3(a) and 3(c), with equally narrow  $\Delta G_S$  peaks of the same sign in each triangle, and in Fig. 3(b), with equally broad  $\Delta G_S$  peaks of opposite sign in each triangle. Linear cuts through these data sets confirm that the line

shapes are identical to within measurement errors. Rearranging Eq. (1) gives the lead asymmetry

$$\Gamma_R/\Gamma_L = (S - 1 - S\alpha)/[1 + (S - 1)\alpha]. \quad (2)$$

From Fig. 3(a), we measure  $\alpha = 0.35 \pm 0.05$ , giving  $\Gamma_R/\Gamma_L = 0.23 \pm 0.08$ . Similar analysis at negative bias [Fig. 3(c)] yields  $\Gamma_R/\Gamma_L = 0.35 \pm 0.10$ . In the positive bias two-electron case [Fig. 3(b)], the hole triangle shows a negative sensor change, indicating that the left barrier is more opaque than the right. It is not possible to further quantify this ratio, as we know from Fig. 2(b) that tunnel rates in the two triangles differ. In this case, unambiguously determining the individual tunnel rates would be possible only by using both charge sensors simultaneously.

In the spin blockade region [Fig. 3(d), near the blue diamond], no sensor variation is seen, confirming that the system is trapped in (1,1). By including lead asymmetry and QPC sensitivities, the rate-equation model used for the insets to Figs. 2(b) and 2(d) yields charge sensor signals as well. These are shown in the insets to Figs. 3(b) and 3(d), and again the agreement is good. The one discrepancy is between the two triangles at negative bias. The model shows a thermally broadened transition from (1,1) to (0,2) at a detuning equal to the bias. This is equivalent to strictly zero interdot tunneling, in which case the system has a ground state and occupations mimic a zero-bias stability diagram. However, between the bias triangles the only mechanism for equilibration is a second order process of each dot exchanging an electron with its lead. This is slow enough to occur on par with the second order and spin-flip processes noted above which circumvent the blockade, so the sensor shows a mixture of (1,1) and (0,2).

### C. Singlet-triplet splitting

Figure 4 illustrates the features that arise at dc bias larger than  $\Delta_{ST}$ , the (0,2) singlet-triplet energy splitting. Panels (a)–(d) show  $I_D$  and  $G_{S2}$  versus voltages  $V_2$  and  $V_6$  at  $\pm 1$  mV bias and a perpendicular magnetic field  $B_\perp = 0.9$  T. At negative bias, spin blockade is lifted when the (1,1) triplet is raised above the (0,2) triplet (pink diagram, +), so in Figs. 4(c) and 4(d), current turns on and steady-state populations shift where  $\Delta > \Delta_{ST}$ , with  $\Delta$  the detuning of the (1,1) ground state with respect to the (0,2) ground state, given by the distance from the upper left side of the triangles. At positive bias, current increases [Fig. 4(a)] and populations shift [Fig. 4(b)] when the Fermi level in the right lead accesses the (0,2) triplet (black diagram,  $\times$ ), which occurs at a fixed distance from the lower left side of each triangle. Thus,  $\Delta_{ST}$  can be measured using either current or charge sensing and either sign of bias, with the energy scale calibrated by equating the triangle size to the dc bias.<sup>12</sup> Current and sensing give consistent values of  $\Delta_{ST}$ , but different splittings are measured at different biases and gate voltages, presumably reflecting real changes in  $\Delta_{ST}$  as these parameters are tuned. The two measurements in Fig. 4(a) give 480 and 660  $\mu$ eV. The negative bias measurement gives  $\sim 520 \pm 50$   $\mu$ eV in Fig. 4(c). The fact that positive bias measurements differ more than negative bias measurements implies that occupation of the left dot has a strong effect on the right dot levels.

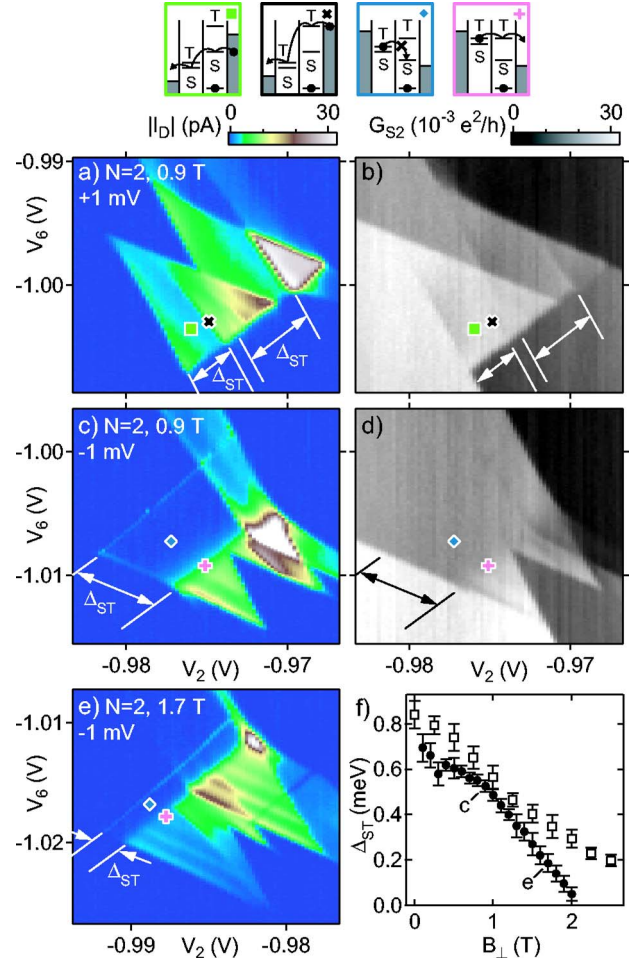


FIG. 4. (Color online) Measurements of the singlet-triplet splitting,  $\Delta_{ST}$ . At +1 mV bias,  $I_D$  (a) and  $G_{S2}$  (b) as a function of  $V_2$  and  $V_6$  at the (1,1)–(0,2) transition show features where triplet current is allowed (black diagram,  $\times$ ) rather than just singlet current (green,  $\blacksquare$ ). At negative bias,  $I_D$  (c) turns on and  $G_{S2}$  (d) changes when triplet states break the spin blockade (pink + vs blue  $\blacklozenge$ ). Several  $\Delta_{ST}$  values are measured from (a) to (d), which we attribute to gate voltage dependence of  $\Delta_{ST}$ . As  $B_\perp$  increases, (e),  $\Delta_{ST}$  decreases rapidly. The dependence of  $\Delta_{ST}$  on  $B_\perp$  is shown in (f), with the solid and open series both taken at negative bias from different gate voltage configurations.

Increasing  $B_\perp$  reduces  $\Delta_{ST}$ , as seen in previous experiments<sup>4,5,15,16</sup> and theoretical work,<sup>16,17</sup> bringing the negative bias current threshold closer to the zero-detuning (upper left) edge. Figure 4(e) shows negative bias current at  $B_\perp = 1.7$  T, where a dramatic decrease in  $\Delta_{ST}$  is seen compared to Fig. 4(c). Figure 4(f) shows  $\Delta_{ST}$  as a function of  $B_\perp$  based on negative-bias data at different gate voltage settings. For the open squares, no voltages besides  $V_2$  and  $V_6$  were changed during the field sweep. The tunnel barriers closed with increasing field, obscuring the measurement above 2.5 T, before the splitting reached zero. The sweep yielding the filled circles and panels (a)–(e), started from different gate voltages and gave  $V_4$  and  $V_{12}$  corrections quadratic in field to keep the barriers roughly constant.  $\Delta_{ST}$  dropped until at 2.1 T no splitting was observed. A split feature was hinted at in the 2.5 T positive bias data, implying that the triplet had

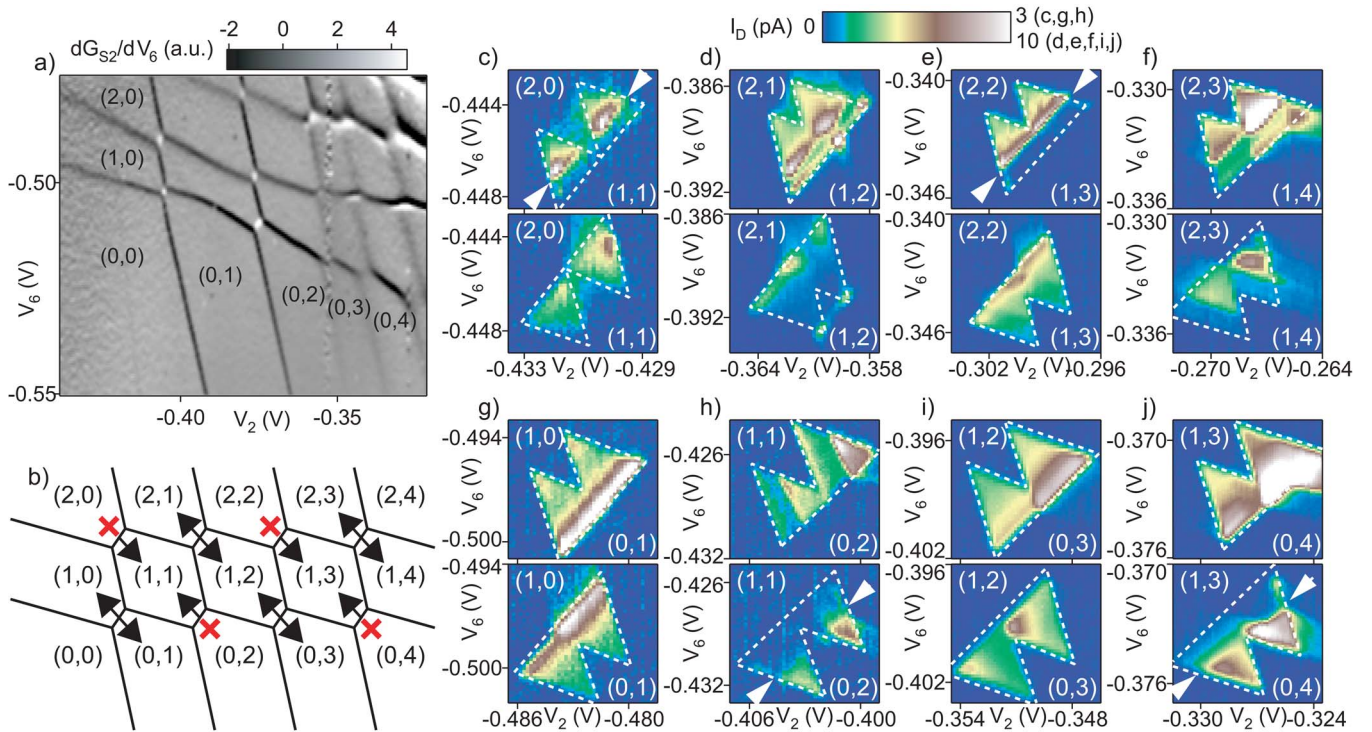


FIG. 5. (Color online) Spin blockade at other charge transitions. (a)  $G_{S2}$  over a wide range of  $V_2$  and  $V_6$ , differentiated numerically in  $V_6$ , maps out the first several charges added to each dot. Bipolar transitions at higher occupation numbers (upper right corner) result from large dot conductance affecting the charge sensor measurement due to the shared drain reservoir. (b) Locations of current suppression due to spin blockade in an even-odd level filling model.  $I_D$  vs  $V_2$  and  $V_6$  at each of these eight transitions for positive (upper half) and negative (lower half) bias are shown in panels (c)–(j). Dashed white outlines are guides to the eye indicating the full bias triangle size. One outline in each panel is drawn by hand, then rotated  $180^\circ$  and overlaid on the opposite bias data to ensure equal size. White arrows indicate the boundaries of observed spin blockade regions.

become the ground state, but again the signal vanished as field increased. Zeeman splitting, though it would be a small effect regardless, is entirely absent at negative bias as interdot transitions connect states with equal Zeeman energy.

#### D. Blockade at other transitions

All of the results so far have concerned two charge transitions, corresponding to adding the first electron to the left dot and either the first or second to the right. Figure 5 extends these measurements through the second charge transition in the left dot (after which the tunnel barriers could no longer be balanced) and through the fourth transition in the right dot (after which complications were observed in the honeycomb pattern, indicative of a triple dot beginning to form). These measurements allow Pauli blockade phenomena to be systematically investigated as one moves toward many-electron systems.

For dots with broken spatial symmetry such that orbital degeneracies are lifted by more than the interaction energies one expects simple even-odd (Pauli) filling of orbital levels, with each odd electron inhabiting a new level and each even electron pairing with the preceding odd electron to form a spin singlet. Figure 5(b) illustrates where one would expect to see spin blockade within this model. When the total number of electrons in the double dot during interdot tunneling is odd, current flows freely in both directions, from one spin

doublet to another, indicated by a double-headed arrow in Fig. 5(b). For even total electron number, one charge state (in which each dot contains an even number of electrons) has a singlet ground state, whereas the other charge state (two odd occupations) may form a triplet or a singlet. Current in one bias direction, indicated by the red (dark gray) X, is therefore expected to be blocked at interdot bias less than the energy gap to the first triplet state in the doubly even charge state. Current at the opposite bias flows freely from one singlet state to the other.

Figure 5(a) shows a large scale plot of the charge sensor signal versus  $V_2$  and  $V_6$ , with zero bias across the dot, differentiated with respect to  $V_6$ . Sharp features in this type of plot mark changes in the occupation of each dot and allow us to determine the absolute occupation at each point. These data were taken after applying positive voltages to the gates while recoiling the same device used in Figs. 1–4 which shifted all charge transitions to less negative gate voltages and gave smaller singlet-triplet splittings. Gates 3, 4, 5, and 12 are adjusted at each charge transition to balance the interdot and dot-lead tunnel barriers. Figures 5(c)–5(j) show current through the dot versus  $V_2$  and  $V_6$  in a field of 100 mT for all charge transitions involving the first or second electron in the left dot and the first through fourth in the right dot—the same transitions shown in Fig. 5(b). The top half of each panel (c)–(j) is measured at positive bias [ $250 \mu\text{V}$  in (c),  $500 \mu\text{V}$  elsewhere] while the bottom half is measured at

an equal negative bias. Spin blockade is seen in each configuration predicted in Fig. 5(b) and nowhere else. At the (1,1) to (0,2) transition [Fig. 5(h)], we measure negative-bias spin blockade as in Figs. 2–4 this time with (0,2) singlet-triplet splitting  $\Delta_{ST} \sim 300 \mu\text{eV}$ . This smaller splitting, compared to the 600–900  $\mu\text{eV}$  seen previously, indicates either a larger and shallower or more elongated potential profile compared with the previous cooldown, such that the energy cost of triplet occupation is decreased. In the mirror-symmetric case, the (1,1) to (2,0) transition [Fig. 5(c)], spin blockade is observed in positive bias, and yields a relatively small (2,0) singlet-triplet splitting of  $\sim 80 \mu\text{eV}$ .

The (1,3) to (2,2) transition [Fig. 5(e)] shows positive bias blockade, as expected for Pauli filling [Fig. 5(b)], with a splitting of  $\sim 140 \mu\text{eV}$ . The blocked (1,3) state is like the (1,1) triplet blockade state found in the two-electron case, with an additional “core” singlet in the right dot. Blockade may be overcome when the (2,2) state with either a triplet in the left dot or in the right dot becomes accessible, so that the measured  $\Delta_{ST}$  represents the minimum of the left-dot and right-dot singlet-triplet splittings.

In zero (and small) field, a two-electron dot always has a singlet ground state,<sup>6</sup> so low-field spin blockade in the two-electron system [Figs. 5(c)–5(h)] will always involve a singlet ground state and triplet excited state. On the other hand, for large numbers of electrons there is no assurance that the ground state is a singlet, even in zero field. For the case of four electrons in a circular potential, for instance, it is known from both theory and experiment that the ground state has spin 1, a consequence of Hund’s rule. This has been observed in a vertical quantum dot through a detailed analysis of the spin transitions seen out to high perpendicular magnetic field,<sup>1</sup> and in a lateral quantum dot comparable in size to one of our dots by the absence of Zeeman splitting in a large parallel field.<sup>18</sup>

In the present system, the observation of spin blockade at the (1,3)–(0,4) transition, Fig. 5(j) ( $\Delta_{ST} \sim 200\text{--}300 \mu\text{eV}$ ) does not allow a determination of the ground state spin of (0,4); only the absolute value of the singlet-triplet splitting of (0,4) is measured. Dependence of the splitting on perpendicular magnetic field also does not determine the ground state spin of (0, 4). For instance, whether the ground state is singlet or triplet, scenarios in which the gap decreases with increasing field can arise.

One piece of evidence suggests that our four-electron dot has a singlet ground state, in contrast to the previous measurements.<sup>1,18</sup> In the (1,4)–(2,3) transition, Fig. 5(f), the (2,3) configuration consists of two singlet pairs and one free spin, making an overall spin-1/2 state. The same is true of (1,4) if the four-electron dot is a singlet, which would not give any current suppression, as observed experimentally. If the four-electron dot were a triplet, the overall (1,4) state could have a spin of either 1/2 or 3/2, leading to a suppression of current from (1,4) to (2,3), which might be termed “doublet-quadruplet spin blockade” when the system gets stuck in a 3/2 state. The absence of spin blockade in Fig. 5(f) leads us to conclude that the four-electron dot is a spin singlet. This observation, contrasting results of previous experiments, may be related to the incipient breakup of the right dot into multiple dots, which occurs at higher electron number. A more systematic investigation of the evolution of spin blockade as electron occupancies increase remains for future work.

#### ACKNOWLEDGMENTS

We acknowledge useful discussions with Jacob Taylor and Amir Yacoby. This work was supported by the ARO under Grant Nos. DAAD55-98-1-0270 and DAAD19-02-1-0070, the DARPA QuIST program, the NSF under Grant No. DMR-0072777, the Harvard NSEC, and iQuest at UCSB.

<sup>1</sup>S. Tarucha, D. G. Austing, T. Honda, R. J. van der Hage, and L. P. Kouwenhoven, *Phys. Rev. Lett.* **77**, 3613 (1996).

<sup>2</sup>J. M. Elzerman, R. Hanson, L. H. W. van Beveren, B. Witkamp, L. M. K. Vandersypen, and L. P. Kouwenhoven, *Nature (London)* **430**, 431 (2004); I. H. Chan, P. Fallahi, A. Vidan, R. M. Westervelt, M. P. Hanson, and A. C. Gossard, *Nanotechnology* **15**, 609 (2004).

<sup>3</sup>M. Ciorga, A. S. Sachrajda, P. Hawrylak, C. Gould, P. Zawadski, S. Jullian, Y. Feng, and Z. Wasilewski, *Phys. Rev. B* **61**, R16315 (2000).

<sup>4</sup>L. P. Kouwenhoven, T. H. Oosterkamp, M. W. S. Danoeastro, M. Eto, D. G. Austing, T. Honda, and S. Tarucha, *Science* **278**, 1788 (1997); A. Kogan, G. Granger, M. A. Kastner, D. Goldhaber-Gordon, and H. Shtrikman, *Phys. Rev. B* **67**, 113309 (2003).

<sup>5</sup>K. Ono, D. G. Austing, Y. Tokura, and S. Tarucha, *Science* **297**, 1313 (2002).

<sup>6</sup>N. W. Ashcroft and N. D. Mermin, *Solid State Physics* (Harcourt, Philadelphia, 1976), Chap. 32.

<sup>7</sup>K. Ono and S. Tarucha, *Phys. Rev. Lett.* **92**, 256803 (2004).

<sup>8</sup>A. C. Johnson, J. R. Petta, J. M. Taylor, A. Yacoby, M. D. Lukin, C. M. Marcus, M. P. Hanson, and A. C. Gossard, *Nature (London)* **435**, 925 (2005); F. H. L. Koppens, J. A. Folk, J. M. Elzerman, R. Hanson, L. H. Willems van Beveren, I. T. Vink, H. P. Tranitz, W. Wegscheider, L. P. Kouwenhoven, and L. M. K. Vandersypen, *Science* **309**, 1346 (2005);

<sup>9</sup>M. Field, C. G. Smith, M. Pepper, D. A. Ritchie, J. E. F. Frost, G. A. C. Jones, and D. G. Hasko, *Phys. Rev. Lett.* **70**, 1311 (1993); L. DiCarlo, H. J. Lynch, A. C. Johnson, L. I. Childress, K. Crockett, C. M. Marcus, M. P. Hanson, and A. C. Gossard, *ibid.* **92**, 226801 (2004).

<sup>10</sup>D. Weinmann, W. Hausler, and B. Kramer, *Phys. Rev. Lett.* **74**, 984 (1995); H. Imamura, H. Aoki, and P. A. Maksym, *Phys. Rev. B* **57**, R4257 (1998); Y. Tokura, D. G. Austing, and S. Tarucha, *J. Phys.: Condens. Matter* **11**, 6023 (1999); M. Ciorga, M. Pioro-Ladriere, P. Zawadzki, P. Hawrylak, and A. S. Sachrajda, *Appl. Phys. Lett.* **80**, 2177 (2002); L. P. Rokhinson, L. J. Guo, S. Y. Chou, and D. C. Tsui, *Microelectron. Eng.* **63**, 147 (2002); A. K. Huttel, H. Qin, A. W. Holleitner, R. H. Blick, K. Neumaier, D. Weinmann, K. Eberl, and J. P. Kotthaus, *Euro-*

- phys. Lett. **62**, 712 (2003); M. Pioro-Ladriere, M. Ciorga, J. Lapointe, P. Zawadzki, M. Korkusinski, P. Hawrylak, and A. S. Sachrajda, Phys. Rev. Lett. **91**, 026803 (2003); M. C. Rogge, C. Fuhner, U. F. Keyser, and R. J. Haug, Appl. Phys. Lett. **85**, 606 (2004).
- <sup>11</sup>J. R. Petta, A. C. Johnson, C. M. Marcus, M. P. Hanson, and A. C. Gossard, Phys. Rev. Lett. **93**, 186802 (2004).
- <sup>12</sup>W. G. van der Wiel, S. De Franceschi, J. M. Elzerman, T. Fujisawa, S. Tarucha, and L. P. Kouwenhoven, Rev. Mod. Phys. **75**, 1 (2003).
- <sup>13</sup>T. Fujisawa, T. H. Oosterkamp, W. G. van der Wiel, B. W. Broer, R. Aguado, S. Tarucha, and L. P. Kouwenhoven, Science **282**, 932 (1998).
- <sup>14</sup>Including the full triplet degeneracy would decrease the calculated current along the blockaded triangle edges by roughly a factor of 2. While we cannot quantitatively fit to the model given the asymmetry between the electron and hole triangles, the current amplitude with no degeneracy does seem correct to better than a factor of 2. One possibility is that the singlet and  $m_s=0$  triplet may be mixed by nuclei (see Ref. 8) making the effective degeneracies of blockaded and unblockaded states equal.
- <sup>15</sup>B. Su, V. J. Goldman, and J. E. Cunningham, Phys. Rev. B **46**, 7644 (1992); R. C. Ashoori, H. L. Stormer, J. S. Weiner, L. N. Pfeiffer, K. W. Baldwin, and K. W. West, Phys. Rev. Lett. **71**, 613 (1993); T. Fujisawa, D. G. Austing, Y. Tokura, Y. Hirayama, and S. Tarucha, Nature (London) **419**, 278 (2002); T. Fujisawa, D. G. Austing, Y. Tokura, Y. Hirayama, and S. Tarucha, J. Phys.: Condens. Matter **15**, R1395 (2003); D. M. Zumbühl, C. M. Marcus, M. P. Hanson, and A. C. Gossard, Phys. Rev. Lett. **93**, 256801 (2004).
- <sup>16</sup>J. Kyriakidis, M. Pioro-Ladriere, M. Ciorga, A. S. Sachrajda, and P. Hawrylak, Phys. Rev. B **66**, 035320 (2002).
- <sup>17</sup>M. Wagner, U. Merkt, and A. V. Chaplik, Phys. Rev. B **45**, R1951 (1992); D. Pfannkuche, V. Gudmundsson, and P. A. Maksym, *ibid.* **47**, 2244 (1993); P. Hawrylak, Phys. Rev. Lett. **71**, 3347 (1993).
- <sup>18</sup>L. H. W. van Beveren, R. Hanson, I. T. Vink, F. H. L. Koppens, L. P. Kouwenhoven, and L. M. K. Vandersypen, cond-mat/0505486.